Bulk Nuclear Properties from Reactions

P. Danielewicz

National Superconducting Cyclotron Laboratory and
Department of Physics and Astronomy,
Michigan State University, East Lansing, MI 48824, USA

November 1, 2018

Abstract

Extraction of bulk nuclear properties by comparing reaction observables to results from semiclassical transport-model simulations is discussed. Specific properties include the nuclear viscosity, incompressibility and constraints on the nuclear pressure at supranormal densities.

1 Introduction

I shall discuss the extraction of bulk nuclear properties from reactions. Of particular interest will be central reactions of heavy nuclei, characterized by a multitude of emitted particles and by a multitude of competing physical effects. These reactions are commonly described in terms of phase-space distributions f that follow the Boltzmann equation:

$$
\frac{\partial f}{\partial t} + \frac{\partial \epsilon_{\mathbf{p}}}{\partial \mathbf{p}} \frac{\partial f}{\partial \mathbf{r}} - \frac{\partial \epsilon_{\mathbf{p}}}{\partial \mathbf{r}} \frac{\partial f}{\partial \mathbf{p}} = \int d\mathbf{p}_2 \int d\Omega' \, v_{12} \frac{d\sigma}{d\Omega'} \left((1 - f_1)(1 - f_2) \right.
$$
$$
\left. \times f_1' f_2' - (1 - f_1')(1 - f_2') f_1 f_2 \right). \tag{1}
$$

Here, $\epsilon(\mathbf{p}, \{f\})$ is the single particle energy. The terms on the l.h.s. of the equation account for the changes of f due to the motion of particles in the average potential field produced by other particles; the particle velocity is $\mathbf{v} = \partial \epsilon / \partial \mathbf{p}$. The r.h.s. of (1) accounts for changes of f due to collisions.

The transport relying on (1) has been quite successful in applications, describing a multitude of measured single-particle spectra, among other. With a confidence stemming from the success of predictions, the transport theory allows for a good insight into the history and mechanism of reactions. The theory is fairly flexible allowing one to include new particles as energy domain changes and to incorporate new collision processes if these become important.

Despite successes of the theory, there are significant uncertainties in the underlying Boltzmann equation. Thus, the dependence of the single-particle

1

energies on momentum and density is generally not known. In terms of the net system energy, the single-particle energies are:

$$\epsilon = \frac{\delta E}{\delta f}, \tag{2}$$

and they relate to particle optical potentials with

$$U_{opt} = \epsilon - \epsilon_{kin}. \tag{3}$$

The cross sections utilized in the collision integral in (1) are usually such as in free-space, but different cross sections may need to be utilized in the medium. An issue may be the very validity of the Boltzmann equation in a dense system. What if the theory is only phenomenological?

The indicated uncertainities represent difficulties but also opportunities to learn about nuclear systems. The opportunities related to uncertainties include e.g. the nuclear equation of state (EOS) generally related to single-particle energies, and the nuclear transport coefficients related to in-medium cross sections. For progress, it is necessary to identify observables from reactions, or combinations thereof, that are sensitive to a specific uncertainty. It is necessary to understand which particular features of the nuclear system are explored in a reaction and why an outcome may be well described in spite of the uncertainties. In the following, I shall give examples of the inference of bulk properties of nuclear matter from comparing the transport results to reaction data, emphasizing the above points.

2 Stopping, Cross Sections and Viscosity

Observables describing stopping of nuclei on each other in reactions might be used to extract information on in-medium cross sections. However, are the cross sections an objective characterization of a system? Can one talk about isolated collisions when the medium is dense and excited so that Pauli principle does not suppress the frequency of collisions? What about macroscopic system properties? Within the Boltzmann description, the cross-sections are related to the viscosity, proportional to the mean free path and inversely proportional to the cross sections:

$$\eta = \frac{5}{9} T \left[\int d\mathbf{p}\, p^2\, f \right]^2 \Big/ \int d\mathbf{p}_1 \int d\mathbf{p}_2 \int d\Omega'\, v_{12} \frac{d\sigma}{d\Omega'}\, q_{12}^4 \sin^2 \theta'$$
$$\times f_1\, f_2\, (1 - f_1')\, (1 - f_2'), \tag{4}$$

with the relative momentum equal to $q_{12} = |\mathbf{p}_1 - \mathbf{p}_2|/2$. When manipulating the cross sections within simulations, one alters the nuclear viscosity and one can hope that stopping observables probe the viscosity even while a link to cross sections remains ambiguous.

The stopping observables utilized for collisions include the linear momentum transfer (LMT) and ERAT. In the LMT measurements, central ($b \sim 0$) mass
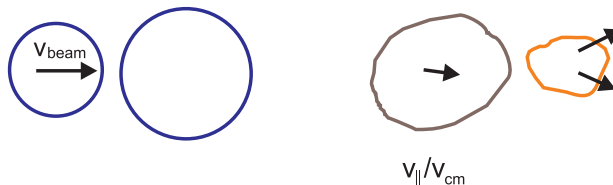
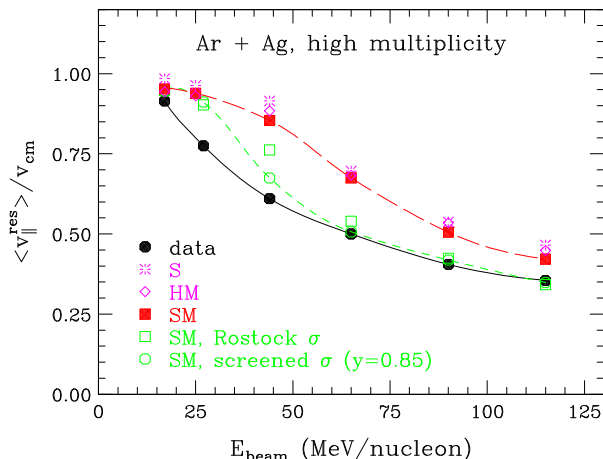Figure 1: A mass-asymmetric collision.

Figure 2: Measured (filled circles) and calculated (other symbols) average velocity ratio $\langle v_\parallel \rangle / v_{cm}$ as a function of beam energy in central ^{40}Ar + Ag collisions.

asymmetric reactions are assessed within the laboratory frame, cf. Fig. 1. The velocity component along the beam of the most massive fragment stemming from a reaction is identified, and its average over reaction events is compared to the cm velocity. A proximity of the average component to the net cm velocity, $\langle v_\parallel \rangle \sim v_{cm}$, indicates fusion in a reaction and, thus, a large level of stopping and, potentially, large elementary cross sections. On the other hand, low values of the average component, $\langle v_\parallel \rangle \sim 0$, indicate little stopping and, potentially, low elementary cross sections.

The Stony Brook group [1] has investigated central ($\langle b \rangle \sim b_{max}/4$) collision events of Ar with several targets, Cu, Ag and Au, and has determined $\langle v_\parallel \rangle / v_{cm}$ as a function of bombarding energy; the results from the Ag target are represented by filled circles in Fig. 2. At low energies, the projectile and target appear to fuse. As energy is raised, the transparency sets in and it increases with the increase in energy. Results of transport simulations assuming free nucleon-nucleon cross sections and different forms of optical potentials are represented, respectively, by stars, diamonds and filled squares in the figure. It is seen that all those calculations overestimate the stopping. The fusion continues too high up in energy and at high energies the residue velocity remains too

high. Notably, the results are rather insentive to the assumed form of nucleon single-particle energies. In consequence, these results point to the in-medium cross-sections reduced compared the free-space, or increased viscosity.

There may be different reasons for an in-medium reduction of cross sections. Thus, it may be reasonable to assume that the geometric cross-section radius should not exceed the interparticle distance,

$$\sigma \lesssim y\,\rho^{-2/3}\,, \tag{5}$$

with $y \sim 1$, since, otherwise, the nucleon-nucleon scatterings can get multiply counted. The requirement may be implemented in practice with the following in-medium cross section:

$$\sigma = \sigma_0 \tanh\left(\sigma_{free}/\sigma_0\right), \qquad \text{where} \qquad \sigma_0 = y\,\rho^{-2/3}\,. \tag{6}$$

There may be other reasons for the cross-section reduction, such as the effects of Pauli principle and of single-particle energy modifications for intermediate states. In the calculations that include those effects (but not the overlap of binary collision regions), such as of the Rostock group [2], a general reduction of the in-medium cross sections is found. In the following, we utilize a crude parametrization of the Rostock cross sections:

$$\sigma = \sigma_{free}\,\exp\left(-0.6\,\frac{\rho}{\rho_0}\,\frac{1}{1+(T_{cm}/150\,\text{MeV})^2}\right) \tag{7}$$

where T_{cm} is the c.m. kinetic energy of a scattering nucleon pair.

The results of the simulations using the two types of reduced in-medium cross-sections are shown in Fig. 2 with open squares and open circles, respectively. It is seen that the stopping is reduced now at higher energies and in a much better agreement with data.

While similar reductions are obtained with the two in-medium cross sections, the two cross sections are actually quite different. This is illustrated in Fig. 3 that shows the number of collisions for the different cross sections, as a function of time. It is seen that the number of collisions for the Rostock cross sections is reduced by $\sim 25\%$ compared to the free cross-sections. However, the number of collisions for the cross sections screened with the interparticle distance is reduced by a factor of 4. How come those two cross sections lead to the same reduction in stopping when the collision numbers are so vastly different?

Clearly, not all collisions are the same. If e.g. the scattering angle in collision is small, the collision may matter little for the reaction dynamics. Notably also such collisions are also most peripheral and most ambigous within a many-body system. In the expression for viscosity (4), the collisions are weighted with the weight $q_{12}^4 \sin^2 \theta'$, suppressing the collisions at low scattering angle, and weighting most those that take place at large relative momentum and lead to θ' $90°$.

While the two different parametrizations of cross sections yield different results regarding the collision number, it is interesting to ask whether they
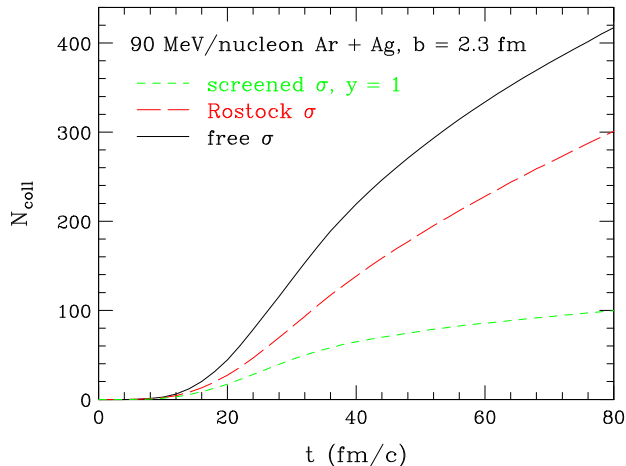
4

Figure 3: Number of collisions in the 90 MeV/nucleon Ar + Ag reaction for different cross sections, as a function of time.

also yield different results for collisions weighted with their importance in the expression for viscosity. This is examined in Fig. 4 and it is seen that the two parametrizations, that yield a right reduction in stopping, also practically agree with regard to the weighted collision number. These parametrizations may be then expected also to agree with regard to an (increased) viscosity of the system.

Another nuclear stopping observable has been the reaction cross section for different values of $ERAT = E_\perp/E_\parallel$, examined in central Au + Au collisions by the FOPI Collaboration [3]. Here, $E_\perp$ and $E_\parallel$ are the transverse and longitudinal energy, respectively. Generally, a value of $ERAT < 2$ indicates a transparency (2 because of two transverse dimensions and only one longitudinal), $ERAT > 2$ indicates a system splashing in the directions transverse to the beam axis, and $ERAT = 2$ indicates isotropy. However, finite-multiplicity fluctuations spread out and modify those results and likewise do the detector inefficiencies. After correcting for the fluctuations and inefficiencies, the FOPI Collaboration concluded that the head-on Au + Au collisions at 250 MeV/nucleon were consistent with isotropy. Figure 5 shows the results for the expected value of $ERAT$ in simulations, with the variation of the inverse of parameter y in the first of our in-medium cross-section parametrizations, together with the result for the second parametrization and for data (with 10% uncertainty). The value of $1/y = 0$ corresponds to free cross sections and these again yield too much stopping. The compatibility with data requires $y \sim 1$. In the analysis, the Rostock and screened cross-section parametrizations yield again very different collision numbers, but similar numbers for collisions entered with viscous weight, when those parametrizations yield a similar stopping. The number of weighted collisions is again reduced by about 30% compared to the case of free cross sections.
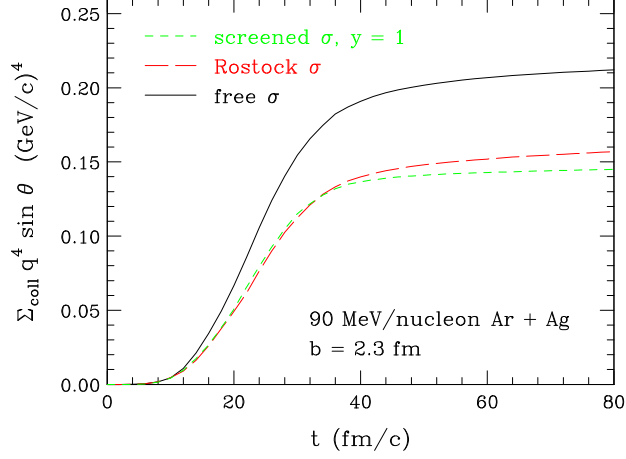
5

Figure 4: Number of collisions weighted with $q^4 \sin^2 \theta$ in the 90 MeV/nucleon Ar + Ag reaction for different cross sections, as a function of time.
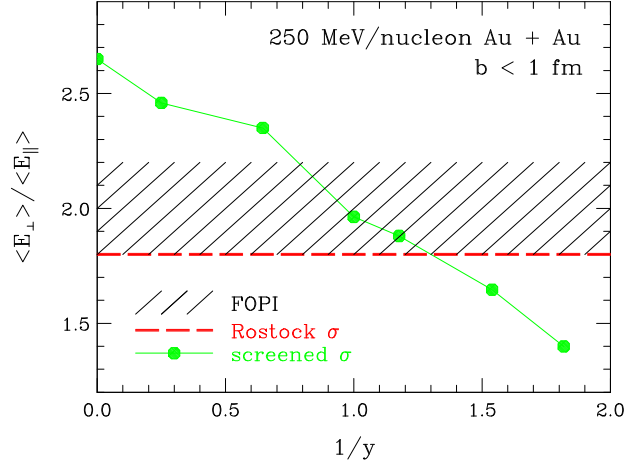

Figure 5: ERAT in central Au + Au reactions at 250 MeV/nucleon. The filled circles represent the results of simulations as a function of the parameter $1/y$ controlling the cross section reduction in (6). The dashed line represents the result of simulations with Rostock cross sections (7). The dashed region represents the data of Ref. [3].
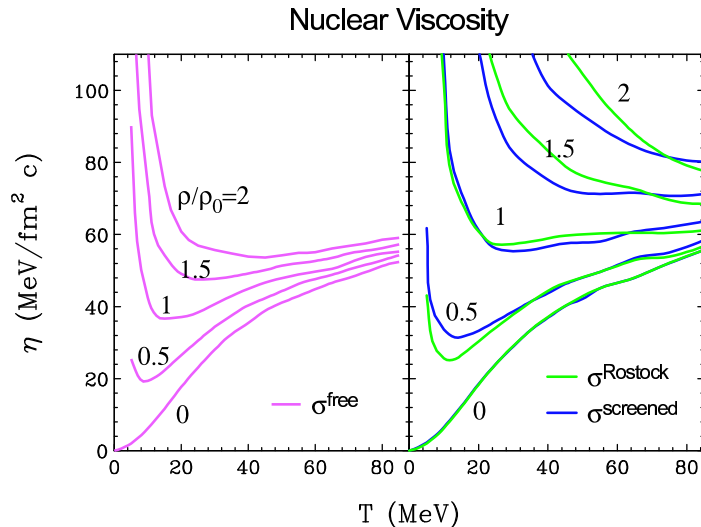
Figure 6: Viscosity in symmetric nuclear matter as a function of temperature T at different densities ρ/ρ_0 for free NN cross sections (left panel) [4] and for medium-modified cross sections (right panel).

Based on the simulations, we can conclude that the stopping observables indicate reduced in-medium cross sections. Details of the reduction appear ambiguous but the stopping primarily appears sensitive to the nuclear viscosity. The very different parametrizations of the cross sections that yield an agreement with data appear relatively consistent with regard to the enhanced nuclear viscosity at densities and temperatures such as explored in the reactions, see Fig. 6. After tackling the viscosity and in-medium cross-sections, we now turn to the features of the nuclear EOS.

3 Nuclear Incompressibility

From the binding-energy formula and from electron scattering, we know that the energy per nucleon in symmetric nuclear matter, under the effects of nuclear forces alone, minimizes at the normal density $\rho_0 = 0.16$ fm^{-3} at -16 MeV. The curvature around the minimum is quantified in terms of incompressibility K, first introduced as a curvature of the energy with respect to the nuclear radius for considered sharp-sphere nuclei,

$$K = 9\,\rho_0^2\,\frac{d^2}{d\rho^2}\left(\frac{E}{A}\right) = R^2\,\frac{d^2}{dR^2}\left(\frac{E}{A}\right)\,. \tag{8}$$

The simplest way to determine the incompressibility may seem to induce volume oscillations in a nucleus. This could be done by scattering α particles off a nucleus, Fig. 7. For the lowest excitation, the excitation energy E^*, deduced
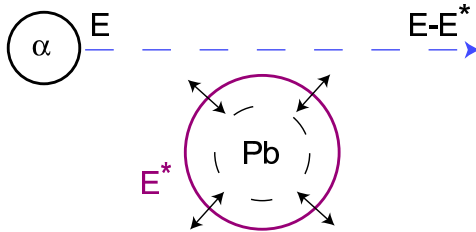
Figure 7: Volume oscillations induced by alpha scattering.

from the final α energy, would be related to the classical frequency through $E^* = \hbar\Omega$, and the latter would be related to K. Let us examine the classical energy of an oscillating nucleus:

$$
\begin{aligned}
E_{tot} &= \int d\mathbf{r}\, \rho\, \frac{m_N\, v^2}{2} + \frac{1}{2}\, A\, K\, (R - R_0)^2 \\
&= \frac{A m_N \langle r^2 \rangle_A \dot{R}^2}{2} + \frac{1}{2}\, A\, K\, (R - R_0)^2\,,
\end{aligned}
\tag{9}
$$

where we use the fact that, for a nucleus uniformly changing its density, the velocity is proportional to the radius, $v = \dot{R}\,(r/R)$. We then obtain the energy of a simple harmonic oscillator; the frequency is a square root of the spring constant divided by mass constant, yielding:

$$
E^* = \hbar\, \sqrt{\frac{K}{m_N\, \langle r^2 \rangle_A}}\,.
\tag{10}
$$

There are complications regarding this reasoning. Thus, the nucleus is not a sharp-edged sphere and the Coulomb interactions play a role in the oscillations in addition to the nuclear interactions different in isospin asymmetric matter than in symmetric. These effects may be accounted for in time-dependent Hartree-Fock or in the random-phase-approximation calculations allowing for meaningful comparisons to data. The above approaches include also shell effects but, if one wants to study just average features of excitations, then the model based on (1) may be employed, provided that the net energy includes contributions from the finite-range of interactions besides Coulomb, isospin and symmetric volume terms [5]. If a nucleus is expanded, by increasing distances from the center by a small fraction, then oscillations result, illustrated in Fig. 8, with a distinct dependence on K. Figure 9 shows next the power spectrum for the oscillations from the Boltzmann equation as well as the 0^+ spectra from precise analyses of alpha scattering [6], in the scattering angle and energy loss. Next, Fig. 10 compares the mass dependence of the resonance energy with the results from the Vlasov equation. The data favor $K = 225 \pm 15$ MeV, represented by the intermediate line.
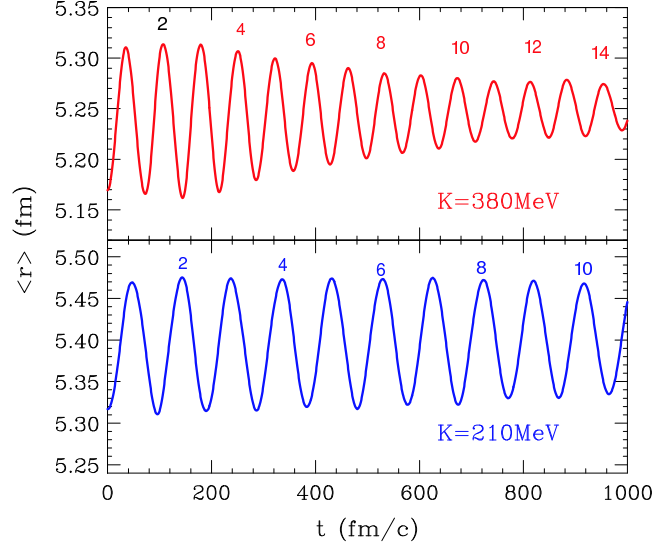
Figure 8: Radius of an expanded lead nucleus as a function of time from the Vlasov version of (1), for two values of incompressibility.
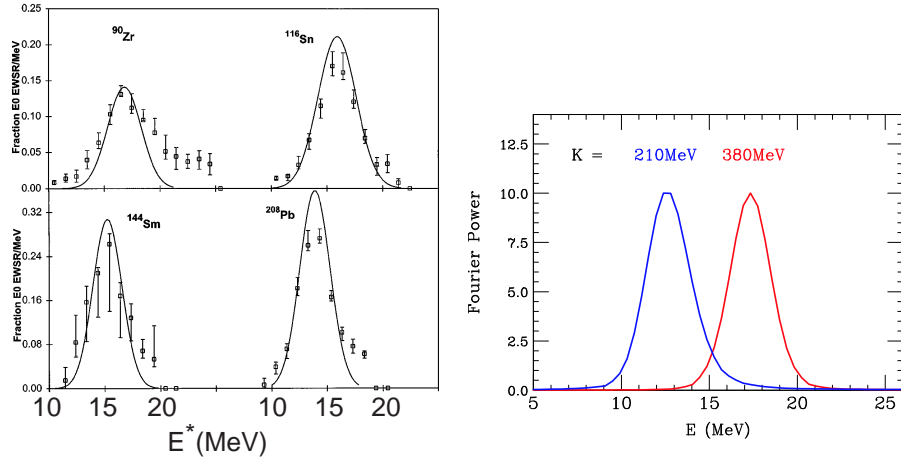

Figure 9: Left: 0^+ excitation spectrum in several nuclei from measurements of Youngblood *et al.* [6]. Right: Fourier spectrum for monopole oscillations in lead within the Vlasov equation for two values of K.
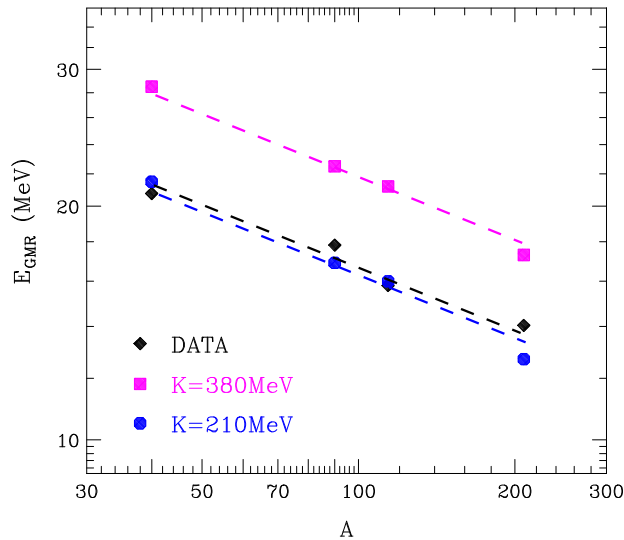
Figure 10: Measured [6] and calculated energies of giant monopole resonances in spherical nuclei.

4 EOS at Supranormal Densities from Flow

Features of EOS at supranormal densities can be inferred from global features of flow in collisions of heavy nuclei at high energies. At low impact parameters, relatively large regions of high density are formed and matter is best equilibrated. The collective flow can provide access to pressure generated in the collision.

To see how the flow relates to pressure, we may look at the hydrodynamic Euler equation for the nuclear fluid, an analog of the Newton equation, in a local frame where the collective velocity vanishes, $v = 0$:

$$(e + p) \frac{\partial}{\partial t} \vec{v} = -\vec{\nabla} p \,. \tag{11}$$

The collective velocity becomes an observable at the end of the reaction. In comparing to the Newton equation, we see that the pressure $p = \rho^2 \frac{\partial(e/\rho)}{\partial \rho}|_{s/\rho}$ plays the role of a potential for the hydrodynamic motion, while the density of enthalpy $w = e + p$ plays the role of a mass. In fact, at moderate energies, the enthalpy density is practically the mass density, $w \approx \rho \, m_N$. We see from the Euler equation that the collective flow can tell us about the pressure in comparison to enthalpy. In establishing the relation, we need to know the spatial size where the pressure gradients develop and this will be determined by the nuclear size. However, we also need the time during the hydrodynamic motion develops and this can represent a problem.

Notably, the first observable that one may want to consider to extract the information on EOS is the net radial or transverse collective energy. That
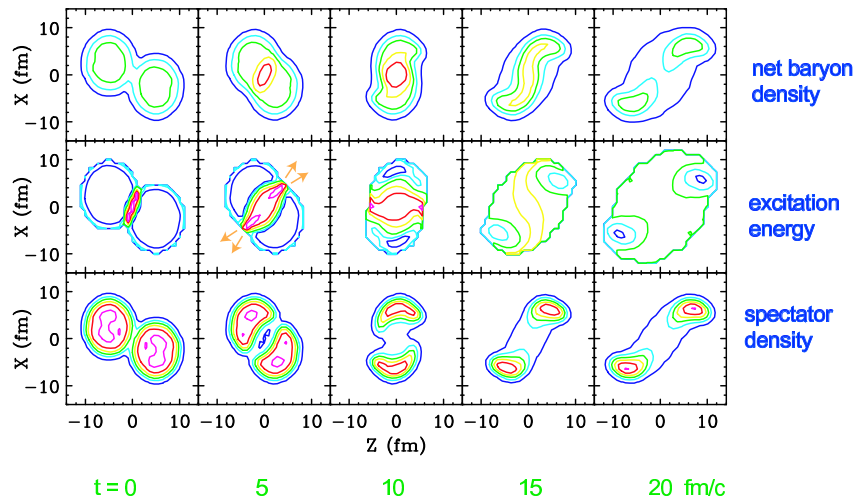
10

Figure 11: Reaction-plane contour plots for different quantities in a ^{124}Sn + ^{124}Sn reaction at 800 MeV/nucleon and $b = 6$ fm, from transport simulations by Shi [7].

energy may reach as much as half of the total kinetic energy in a reaction. Despite its magnitude, the energy is not useful for extracting the information on EOS because of the lack of information on how long the energy develops. Large pressures acting over a short time can produce the same net collective energy as low pressures acting over a long time. This makes appearent the need for a timer in reactions.

The role of the timer in reactions may be taken on by the so-called spectators. The spectator nucleons are those in the periphery of an energetic reaction, weakly affected by the reaction process, proceeding virtually at undisturbed original velocity, see Fig. 11. Participant nucleons, on the other hand, are those closer to the center of the reaction, participating in violent processes, subject to matter compression and expansion in the reaction. As the participant zone expands, the spectators, moving at a prescribed pace, shadow the expansion. If the pressures in the central region are high and the expansion is rapid, the anisotropies generated by the presence of spectators are going to be strong. On the other hand, if the pressures are low and, correspondingly, the expansion of the matter is slow, the shadows left by spectators will not be very pronounced.

There are different types of anisotropies in the emission that the spectators can produce. Thus, throughout the early stages of a collisions, the particles move primarily along the beam axis in the center of mass. However, during the compression stage, the participants get locked within a channel, titled at an angle, between the spectator pieces, cf. Fig. 11. As a consequence, the forward and backward emitted particles acquire an average deflection away from the beam axis, towards the channel direction. Another anisotropy is the ellipticity
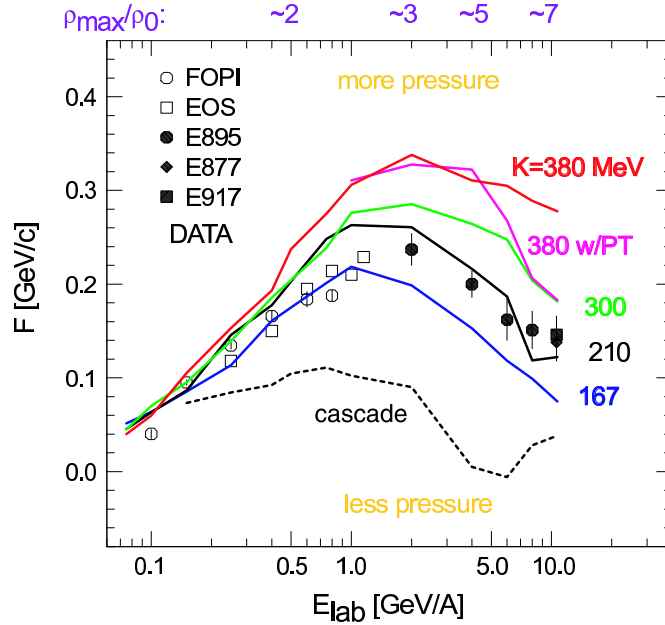
11

Figure 12: Sideward flow excitation function for Au + Au. Data and transport calculations are respresented, respectively, by symbols and lines [8].

v_2, that we already examined as a function of $p^\perp$ in midperipheral collisions. Now we will consider global v_2 values at lower impact parameters.

The different anisotropies have been quantified experimentally over a wide range of bombarding energies in Au + Au collisions. Figure 12 shows the measure of the sideward forward-backward deflection as a function of the beam energy, with symbols representing data. Lines represent simulations assuming different EOS. On top of the figure, typical maximal densities are indicated which are reached at a given bombarding energy. Without interaction contributions to pressure, the simulations labelled cascade produce far too weak anisotropies to be compatible with data. The simulations with EOS characterized by the incompressibility $K = 167$ MeV yield adequate anisotropy at lower beam energies, but too low at higher energies. On the other hand, with the EOS characterized by $K = 380$ MeV, the anisotropy appears too high at virtually all energies. It should be mentioned that the incompressibilities should be considered here as merely labels for the different utilized EOS. The pressures resulting in the expansion are produced at densities significantly higher than normal and, in fact, changing in the course of the reaction.

Figure 13 shows next the anisotropy of emission at midrapidity, with symbols representing data and lines representing simulations. Again, we see that without interaction contributions to pressure, simulations cannot reproduce the measurements. The simulations with $K = 167$ MeV give too little pressure at
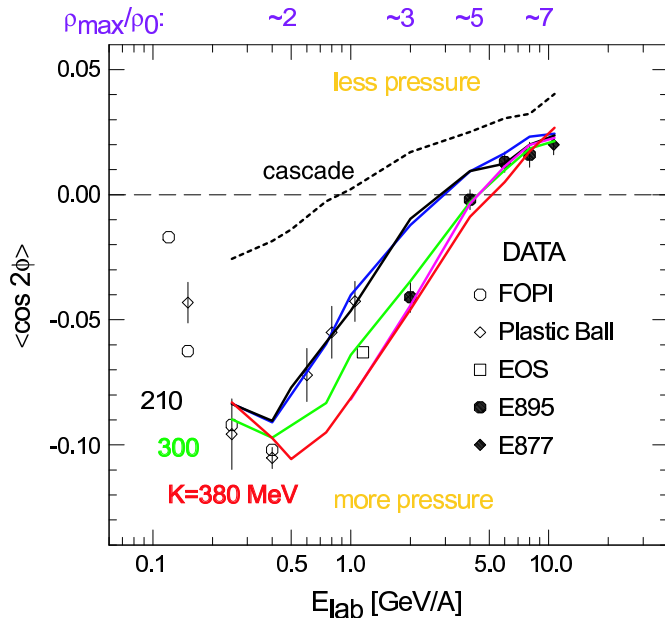
Figure 13: Elliptic flow excitation function for Au + Au. Data and transport calculations are respresented, respectively, by symbols and lines [8].

high energies, and those with $K = 380$ MeV generally too much. A level of discrepancy is seen between data from different experiments.

We see that no single EOS allows for a simultaneous description of both types of anisotropies at all energies. In particular, the $K = 210$ MeV EOS is the best for the sideward anisotropy, and the $K = 300$ MeV EOS is the best for the elliptic anisotropy. We can use the discrepancy between the conclusions drawn from the two types of anisotropies as a measure of inaccuaracy of the theory and draw broad boundaries on pressure as a function of density from what is common in conclusions based on the two anisotropies. To ensure that the effects of compression dominate in the reaction over other effects, we limit ourselves to densities higher than twice the normal. The boundaries on the pressure are shown in Fig. 14 and they eliminate some of the more extreme models for EOS utilized in nuclear physics, such as the relativistic NL3 model and models assuming a phase transition at relatively low densities, cf. Fig. 15.

5   Conclusions and Outlook

Comparisons of transport model calculations to data can yield information on bulk nuclear properties. However, the progress has been difficult due to the need to sort out competing physical effects. Optimal observables are those which are mostly sensitive to one uncertain nuclear property.
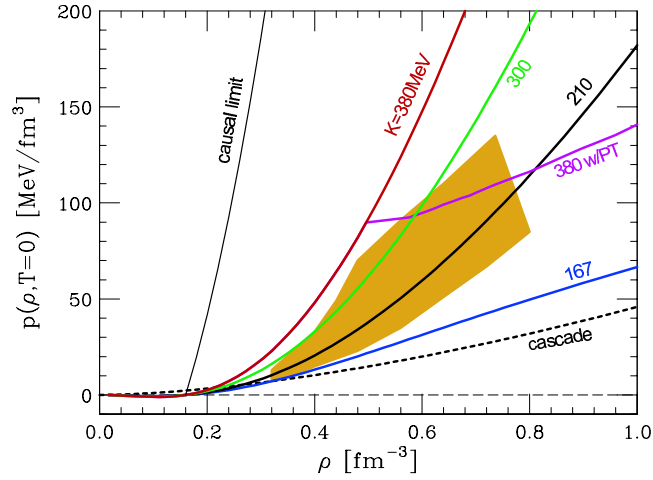
13

Figure 14: Constraints from flow on the $T = 0$ pressure-density relation, indicated by the shaded region [8].
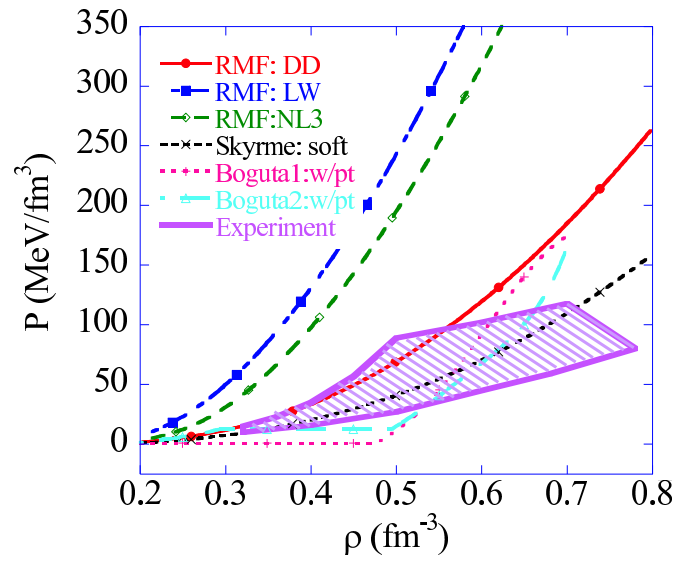

Figure 15: Impact of the constraints on models for EOS [8].

Though the stopping observables are sensitive to the in-medium cross sections, they probe cross sections weigthed with scattering angle, such as appear in the expression for nuclear viscosity. These appear reduced in lower-energy reactions by ~ 30 % compared to free space and the nuclear viscosity appears increased respectively by ~ 50 % compared to that calculated with free cross sections.

Most straightforward determination incompressibility is by analyzing the excitation of density oscillations. The far more precise measurements of giant monopole resonances than in the past suggest a value $K \sim 225$ MeV.

The flow in energetic reactions allows to place meanigful constraints on the nuclear pressure within the density range $2 \lesssim \rho/\rho_0 \lesssim 5$. The most extreme models for EOS can be eliminated.

Acknowledgement

References

[1] E. Colin *et al.*, Phys. Rev. C 57 (1998) R1032; R. Sun *et al.*, to be published.

[2] H.-J. Schulze *et al.*, Phys. Rev. C 55 (1997) 3006; A. Schnell *et al.*, Phys. Rev. C 57 (1998) 806.

[3] W. Reisdorf *et al.*, Nucl. Phys. A612 (1997) 193.

[4] P. Danielewicz, Phys. Lett. B 146 (1984) 168.

[5] P. Danielewicz, Nucl. Phys. A673 (2000) 375.

[6] D. H. Youngblood, Nucl. Phys. A687 (2001) 1c.

[7] L. Shi *et al.*, Phys. Rev. C 64 (2001) 034601.

[8] P. Danielewicz *et al.*, submitted for publication.